Icarus 311 (2018) 135–145

Contents lists available at ScienceDirect

Icarus

journal homepage: www.elsevier.com/locate/icarus

Europa's ice-related atmosphere: The sputter contribution

A. Vorburger*, P. Wurz

Physikalisches Institut, University of Bern, Bern, Switzerland

ARTICLE INFO

Article history:
Received 25 July 2017
Revised 21 January 2018
Accepted 21 March 2018
Available online 27 March 2018

Keywords:
Europa
Exosphere
Monte-Carlo model
Ice sputtering
JUICE

ABSTRACT

Europa, Jupiter's innermost icy satellite, is embedded well within Jupiter's magnetospheric plasma, an intense flux of ions and electrons that approximately co-rotate with Jupiter. The plasma can be thought of as consisting of two populations: The cold, thermal plasma containing charged particles with energies ranging from 1 eV to 1 keV, and the hot, energetic plasma containing charged particles with energies ranging from 10 keV to 100 MeV. When the charged particles interact with Europa's surface, they not only chemically and physically alter the icy surface, but also liberate material from the surface through a process called sputtering, which in turn forms a tenuous atmosphere.

In this paper we calculate the sputter contribution to the atmosphere by modeling the formation of Europa's ice-sputtered atmosphere ab initio. We consider the species H, H_2, O, OH, H_2O, O_2, HO_2, H_2O_2, and O_3, all of which are related to the water–ice surface. Whereas the ice sputter yields of H2O, H2, and O2 have been well established, the ice sputter yields (and the resulting density profiles) of H, O, OH, HO_2 and O_3 are small and largely unknown. As model input we use available plasma ion and electron energy spectra as well as available water-ice sputter yields. Based on first principles, i.e., without applying any scaling to observed data, we calculate atmospheric densities ab initio.

Our results match available observational data and previously published modeling efforts well. Europa's exosphere is dominated by thermally accommodated O_2 close to the surface (below a few 100 km), and the much lighter H_2 molecules at higher altitudes. The water-ice related species that stick to the surface (freeze out) are liberated by cold and hot plasma sputtering in about equal amounts. In addition, in the case of H_2, O_2, and H_2O_2, electrons contribute almost as significantly to the sputter yield as ions do.

1. Introduction

Europa's orbit is located at an average distance of 9.38 R_J from Jupiter (where R_J is Jupiter's radius, or 71,400 km) and nearly coincides with Jupiter's equatorial plane. The moon's orbit thus lies well inside the jovian magnetopause, which is typically located at 60–100 R_J (Joy et al., 2002), and at the outer edge of the Io plasma torus. Jupiter's magnetospheric plasma approximately co-rotates with Jupiter, lagging only marginally behind Jupiter's rotation period of ~10 h, thus traveling at an average speed of ~90 km/s at Europa's orbital distance. Europa's orbital speed of ~14 km/s is substantially lower than the azimuthal plasma velocity, resulting in the plasma flowing over the moon from it's trailing hemisphere and sweeping ahead of it in its orbital motion with a relative speed of ~76 km/s. Whereas the main part of the Jovian plasma consists of this cold, thermal plasma, there is a second population, termed the hot, energetic plasma. This plasma has been accelerated to energies surpassing 10 keV, and, while it is quite sparse, it contains most of the overall energy flux.

As the Jovian plasma encounters Europa's surface, two important processes are induced: radiolysis and sputtering. Radiolysis is the dissociation of molecules into fragments by ionizing radiation inside the ice. Since the resulting fragments are mostly radicals they are chemically reactive, and will recombine to form new, more stable, species in the ice. The second process, sputtering, is the ejection of particles from a solid surface due to its bombardment by energetic particles. The number of ejected particles depends on the plasma flux, the plasma energy, the plasma composition, the plasma charge state, the plasma incidence angle, and the surface temperature.

In the theoretical formulation, the sputter yield is a function of an ion's stopping power, i.e., the energy per length that is deposited as the ion passes through a solid (Betz and Wehner, 1983). At higher energies, the stopping power linearly increases with velocity up to ~300 keV/nuc, above which it starts to decrease again. Several sputter experiments on ice have been conducted to determine the sputter yield of water ice (the number of ejected H_2O molecules per incident ion) for various ion species at various ener-

* Corresponding author.
E-mail address: avorburger@space.unibe.ch (A. Vorburger).

https://doi.org/10.1016/j.icarus.2018.03.022
0019-1035/

gies. See Cassidy et al. (2013), Fig. 3, for a compilation of available water sputter yield data and theory. Recently, first sputter yield measurements for electrons sputtering water ice were presented by Galli et al. (2017).

In this paper we calculate ab initio the contributions to the exosphere by sputtering of water ice by cold and hot plasma ions and electrons. Available observations of Europa's water ice related atmosphere are presented in Section 2. The Monte Carlo model, including plasma parameters and sputter yields, are presented in Section 3. The results of our Monte Carlo simulation are presented in Section 4, and a comparison with available observations and previous models is given in Section 5. Section 6, the conclusion section, completes this paper.

2. Available observations

Very little is known about the chemical composition of Europa's atmosphere from observations (see recent review by McGrath et al., 2009). The only presently confirmed exospheric constituents consist of its main component O and O_2, the alkali metals Na and K, H_2O (in form of plumes), and, detected most recently, a H corona. Whereas O_2 and H_2O was not directly observed, their presence was inferred from O and H observations. The following subsections give an overview of present-day available observations of Europa's water ice related atmosphere.

2.1. O and O_2

Hall et al. (1995) detected O I 1304 Å and O I 1356 Å air-glow emissions in Europa's exosphere using the Goddard High Resolution Spectrograph (GHRS) on the Hubble Space Telescope (HST) during six consecutive spacecraft orbits in June 1994. Their measurements yield an O I 1356 Å–1304 Å atmospheric emission ratio of 1.9, implying electron dissociation excitation of O_2 as the responsible emission process, since this is the only process known to produce a brighter 1356 Å than 1304 Å line. Through atmospheric modeling the authors derive an O_2 column density of $N_C(O_2) = (1.5 \pm 0.5) \cdot 10^{15}$ cm^{-2} and a 2.5 σ upper limit for the O column density of $N_C(O) < 2 \cdot 10^{14}$ cm^{-2}.

Three years later, Hall et al. (1998) presented two more sets of HST/GHRS observations of Europa's exosphere made in June 1996 and July 1996. Complete analysis of HST/HGRS observations yield air-glow emission ratios between 1.3 and 2.2. Assuming both a uniform atmosphere and a spatially uniform electron impact excitation rate, the authors derive O_2 column densities of $N_C(O_2) = (2.4–14) \cdot 10^{14}$ cm^{-2} and 3 σ upper limits for the O column density of $N_C(O) < (1.6–3.4) \cdot 10^{13}$ cm^{-2}.

In 1999, McGrath et al. (2004) obtained 9 images of Europa's trailing hemisphere from the Space Telescope Imaging Spectrograph (STIS) on board HST. Surprisingly, the O I atomic emission 1356 Å peaks within the disk and not at the limb of the satellite, as would be expected from plasma interaction with an optically thin atmosphere. In addition, the images include a brighter region on the antijovian hemisphere, i.e., the emission is spatially inhomogeneous, probably due to the surface not being icy to the same degree everywhere.

Hansen et al. (2005) observed the O multiplet of lines with Cassini's Ultra-Violet Imaging Spectrograph (UVIS) on two different dates in January 2001. Their measurements are best fit by a bound, near-surface O_2 atmosphere with a scale height of ~200 km and an O atmosphere consisting of a loosely bound component showing the spectral character of a point source and a diffuse component, which overfills one pixel (~7 R_E, where R_E is equal to Europa's radius of 1569 km). From their measurements the authors derive atomic and molecular oxygen densities and column densities, and an $O/(O + O_2)$ ratio of 0.02.

Four more sets of UV observations of Europa were taken in spring 2007 by the HST Wide-Field Planetary Camera 2 (WFPC2), by the HST Advanced Camera for Surveys (ACS), and by New Horizons' Alice UV imaging spectrograph (Retherford et al. (2007). See also McGrath et al. (2009) and references therein). While the WFPC2 images do not reveal any measurable atmospheric emissions, the ACS images contain emissions at 1304 Å and 1356 Å on the subjovian hemisphere. Unfortunately, the latter images are difficult to interpret due to detector dark noise and due to the uncertainty of Europa's location within the images. The Alice measurements also cover emissions at 1304 Å and 1356 Å, confirming the value of ~2 for the 1356 Å to 1304 Å ratio, again suggesting an O_2 dominated atmosphere.

In 2011 Saur et al. (2011) presented five previously unpublished HST/ACS measurements taken in June 2008. While the authors did not find any asymmetry in the atmospheric emission with respect to the sub-Jovian/anti-Jovian side, they did find a surplus of emission near 90° west longitude. Making similar assumptions as Hall et al. (1995), Saur et al. (2011) derive a lower limit of the O_2 column density of $N_C(O_2) > (6–10) \cdot 10^{14}$ cm^{-2}. These measurements are generally compatible with previous observations, being slightly smaller than the fluxes obtained with HST/STIS by McGrath et al. (2004, 2009) but in the range or slightly larger than previous HST/GHRS observations.

Most recently, Roth et al. (2016) presented a comprehensive set of HST observations of Europa's far ultraviolet oxygen aurora. The measured O I 1356Å to 1304Å flux ratio of 1.5–2.8, with a mean of 2.0, agrees well with previously published ratios, supporting the conclusion that Europa's bound atmosphere is dominated by O_2. Generally, the oxygen ratio decreases with increasing distance from the surface, with O_2 prevailing over O up to ~900 km. The authors divided the data into three regions (near-surface up to 1.25 R_E, high altitude from 1.25 R_E to 1.5 R_E, and corona from 1.5 R_E to 1.6 R_E) and derive O/O_2 mixing ratios of 0.01–0.06, 0.13–0.15, and 0.27–0.35, for the three altitude regions. Considering various aspects of the variable plasma environment and the atmospheric distribution, the authors derive O_2 column densities of $N_C(O_2) = (3–6) \cdot 10^{14}$ cm^{-2}. The variable mixing ratio is suggesting largely different scale heights for the O and O_2 exospheric components.

2.2. H

Recently, Roth et al. (2017) reported on the first observations of an atomic hydrogen corona extending up to several moon radii above the limb of Europa. The observations were taken by STIS onboard the HST on six occasions between December 2014 and March 2015. The observations agree well with a radially escaping H corona with maximum densities at the surface of $N(H) = (1.5–2.25) \cdot 10^3$ cm^{-3}, with an average of $N(H) = 1.8 \cdot 10^3$ cm^{-3}, and a line-of-sight $1/r$ profile. The fitted densities vary by ±20% for the six observations, which exceeds the obtained uncertainties. The authors thus concluded that an intrinsic variability of the H corona must exist.

2.3. H_2O

In 2014 Roth et al. (2014) reported on statistically significant coincident excess of hydrogen Lyman-α and oxygen 1304 Å emissions above Europa's southern hemisphere measured by HST/STIS. These highly variable emission excesses suggest a local atmospheric H_2O enhancement, most probably a 200 ± 100 km high water plume located on the anti-Jovian southern hemisphere. The authors derive average H_2O and O_2 column densities using measured cross sections for electron-impact dissociative excitation and standard plasma parameters for Europa. Their analysis yields an O_2 column density of $N_C(O_2) \sim 5 \cdot 10^{15}$ cm^{-2} and a H_2O column density of

$N_C(H_2O) = 1.5{\cdot}10^{16}$ cm^{-2}. This signal is by a factor of 100–1000 larger than in the regular atmosphere.

3. Modeling approach

Europa's atmosphere presented herein is modeled ab initio, i.e., no fitting to observations of the exosphere was applied. The calculation starts at the exobase that we assume to be Europa's surface. No assumption on the sputtered neutral particle flux or on neutral column densities are made. Instead, the only inputs required are the parameters describing the plasma particle flux onto the surface (presented in Section 3.2) and the parameters describing the ice-related neutral sputter yield (presented in Section 3.3).

3.1. Monte Carlo model

The exospheric density profiles presented herein were calculated with a Monte Carlo code originally developed for studying Mercury's exosphere (Wurz and Lammer, 2003). In this model, the trajectories of a large amount of particles are computed independently (i.e., the model is collision-free) ab initio. Each sputtered particle starts its trajectory at the exobase (which in this case is assumed to be Europa's surface), with an energy E sampled randomly from the energy distribution for sputtered particles:

$$f(E) = \frac{6E_b}{3 - 8\sqrt{E_b/E_c}} \frac{E}{(E+E_b)^3} \left(1 - \sqrt{\frac{E+E_b}{E_c}}\right), \quad (1)$$

where E_b is the surface binding energy, and E_c is the maximum energy that can possibly be transferred in a binary collision between the impacting particle and the surface atom.

Each sublimated, or thermally accommodated, particle also starts its trajectory at the exobase, but with an energy sampled randomly from a Maxwellian distribution around the thermal energy $E_T = k_B T$:

$$f(E) = 2\sqrt{\frac{E}{\pi}} \left(\frac{1}{k_B T}\right)^{3/2} \exp\left(\frac{-E}{k_B T}\right) \quad (2)$$

where k_B is the Boltzmann constant, and T is the surface temperature.

Similarly, the particle's ejection angles from the surface are obtained by randomly sampling two angular distribution functions, one for the polar angle and one for the azimuth angle. For the polar angle (θ) dependence we use a cosine function, which was found to best describe sputtering from a porous regolith (Cassidy and Johnson, 2005). For the azimuth angle (ϕ) we use a uniform distribution over 2π.

Having obtained an initial velocity vector, a particle's elliptic or hyperbolic trajectory is calculated according to Equations 8 through 17 in Hodges (1994). Whereas we compute the velocities in 2D (i.e., in the radial and tangential direction), we only monitor the particle's position in the radial direction. Trajectories are computed until the particle either leaves the calculation domain (which in our model is given by Europa's Hill radius, or 12,084 km), gets ionized (see Section 3.4), is fragmented (upon which the fragments are traced instead, see also Section 3.4), or falls back to the surface. Particles that return to the surface are assumed to be either completely sticking (H, O, OH, H_2O, HO_2, H_2O_2, O_3) or completely non-sticking (O_2 and H_2).

From the calculated trajectories we derive exospheric neutral density profiles and radial column densities by multiplying the simulated profiles with the exobase density. For each species (i) and each release process (p), the exobase density N_i^p (in (m^{-3})) is obtained by dividing the process specific surface release flux Φ_i^p (in ($m^{-2}s^{-1}$)) by the particles' mean initial velocity $\langle v_i^p \rangle$ (in (m/s)):

$$N_i^p = \Phi_i^p / \langle v_i^p \rangle. \quad (3)$$

The mean initial velocity is computed from the energy distribution given in Eqs. (1) and (2), whereas the surface release flux is computed from the energy dependent plasma flux $\Phi_{\text{plasma}}(E)$, the species dependent surface fraction f_i, and the energy dependent sputter yield $Y(E)$:

$$\Phi_i^{sp} = \int \Phi_{\text{plasma}}(E) \cdot f_i \cdot Y(E) dE, \quad (4)$$

in the case of sputtered particles, and from the vapor pressure in the case of sublimated and thermally accommodated particles:

$$\Phi_i^{th} = f_i \cdot \frac{p_0}{k_B T} \cdot \sqrt{\frac{8 k_B T}{\pi m}}, \quad (5)$$

where f_i is the surface fraction of species i, p_0 is the temperature specific water vapor pressure, k_B is the Boltzmann constant, T is the surface temperature, and m is the particle mass of species i.

3.2. Jovian plasma

The jovian plasma can be thought of as consisting of two populations: The cold, thermal plasma, and the hot, energetic plasma. Whereas the two plasma populations are described in detail below, an overview of the relevant plasma parameters and a depiction of the plasmas' spectral shapes can be found in Table 1 and Fig. 1, respectively.

The cold, thermal plasma has been described extensively in Kivelson et al. (2009) and Bagenal et al. (2015). The ion composition mainly includes oxygen, sulfur and hydrogen, with relative abundances of H^+:O^{n+}:S^{n+} = 1:3:1.7 (Bagenal et al., 2015). These relative abundances result in an average ion mass of 18.14 amu, which agrees well with the value of 18.5 amu given by Kivelson et al. (2009). The electron density is slightly higher than the ion density, with average values for electrons of 150 cm^{-3} and for ions of 130 cm^{-3}. Plasma modeling has shown that due to the electro-magnetic field conditions in the vicinity of Europa the cold, thermal plasma is to a significant extent deflected around Europa, decreasing the flux of particles impinging onto the surface (see e.g. Saur et al., 1998 and Rubin et al., 2015). Based on the results from model calculations, we implement a reduction of the cold plasma flux onto the surface by 80%. The energy spectrum of the cold plasma exhibits roughly the shape of a Maxwellian distribution, with a mean drift velocity of 90 km/s, an ion temperature of ~100 eV, and an electron temperature of ~20 eV. With Europa orbiting Jupiter at an orbital velocity of 14 km/s, the plasma's velocity relative to the moon is reduced by 14 km/s, i.e., the plasma sweeps over Europa's trailing hemisphere at a relative speed of 76 km/s. Since the plasma temperature is of the same order of magnitude as the plasma bulk speed, it is non-negligible and has to be taken into account when modeling the plasma interaction with Europa's surface. For this study the cold plasma was thus modeled by a drifting Maxwellian distribution, with a 1D drift velocity of 76 km/s, and a temperature of 100 eV and 20 eV for the ions and electrons of the cold plasma, respectively.

Characteristics of the hot plasma ions have been presented in detail in Divine and Garrett (1983), Cooper et al. (2001), Paranicas et al. (2002) and Mauk et al. (2004), while characteristics of the hot plasma electrons were presented in Paranicas et al. (2001). As already implied by the term 'hot', the temperature of the electrons and ions of this plasma group is quite high, ranging from a few keV to a few MeV. The energy spectrum of the hot ions is generally modeled by a kappa distribution with characteristic energies of a few tens to hundreds of keV, and a power-law tail representing the radiation belt ions. For

Table 1
Characteristic parameters for the cold and hot plasma. Given are rounded mean values assembled from Bagenal et al. (2015); Paranicas et al. (2002); Mauk et al. (2004).

	Density (cm^{-3})	v_{drift} (km/s)	v_{kT} (km/s)	E_{char} (eV)	E_{kT} (eV)	Flux ($m^{-2}s^{-1}$)
Cold plasma						
e^-	150	76	3000	0.016	20	$1.2{\cdot}10^{13}$
i^+						
H^+	23	76	139	30	100	$1.7{\cdot}10^{12}$
O^{n+}	68	76	35	479	100	$5.2{\cdot}10^{12}$
S^{n+}	39	76	25	958	100	$3.0{\cdot}10^{12}$
Hot plasma						
e^-				50,000	1000	$1.5{\cdot}10^{12}$
i^+						
H^+				250,000	30,900	$7.5{\cdot}10^{10}$
O^{n+}				140,000	17,200	$4{\cdot}10^{10}$
S^{n+}				120,000	17,200	$8{\cdot}10^{10}$

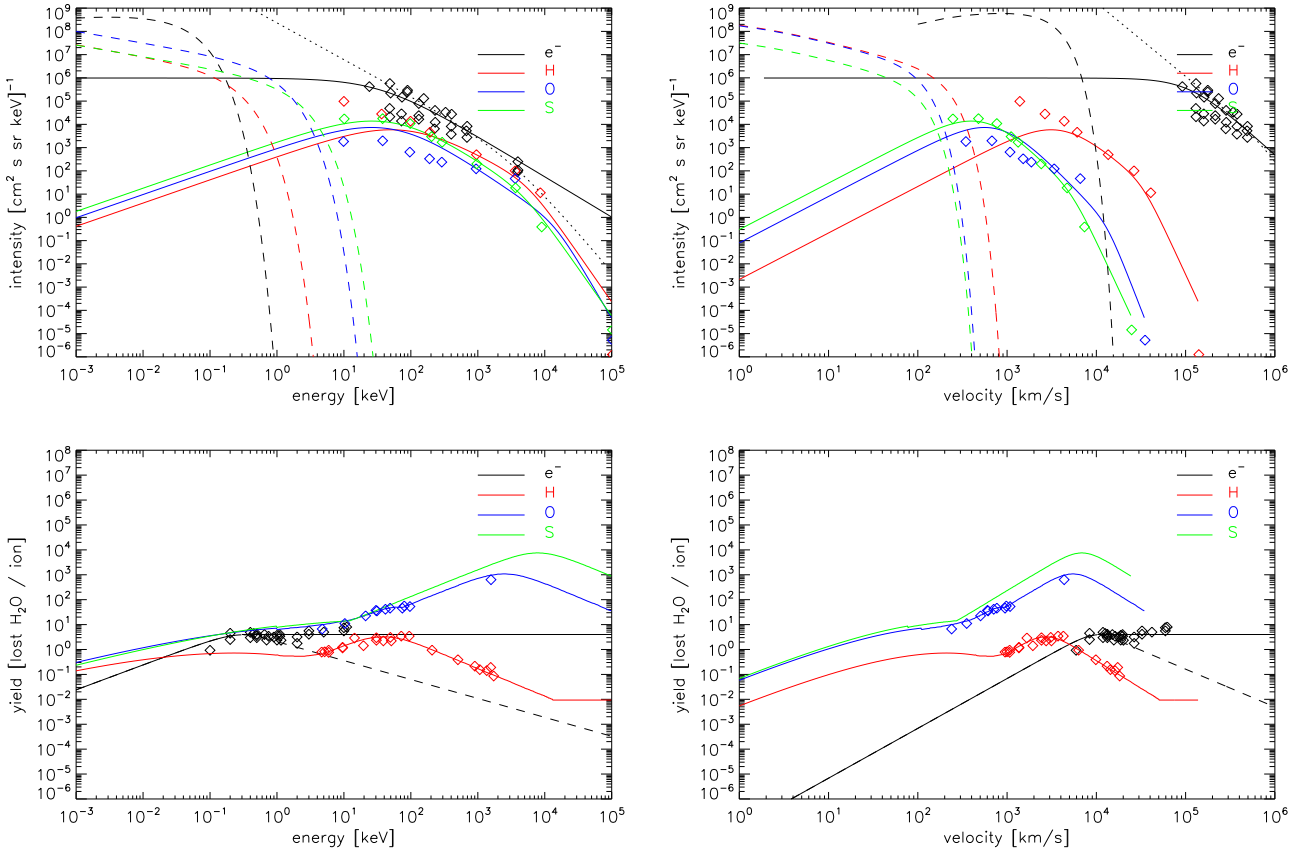

Fig. 1. Measurements and fits for the cold and hot plasma ions and electrons (top) and water sputter yields (bottom) as a function of energy (left) and velocity (right). Ion intensity measurements (top; red, blue, and green diamonds) were taken from Ip et al. (1998) whereas electron intensity measurements (top; black diamonds) were taken from Paranicas et al. (2001). The energy spectra of the cold plasma were fitted with drifting Maxwellian distributions (top; dashed lines) whereas the hot plasma energy spectra were fitted with Kappa distributions (top; solid lines). Also shown, for comparison, is the electron spectral shape as presented in Paranicas et al. (2001) (top; dotted black lines). The sputter yield measurements combine results collected in Cassidy et al. (2013) (H^+ and O^+) and experimental results from Galli et al. (2017) (electrons). The ion sputter curves are a combination of the equations published by Famá et al. (2008) and Johnson et al. (2009), whereas for the electrons we show the sputter yield curve as given by Teolis et al. (2017) (bottom; black dashed lines) and as implemented herein (bottom; black solid lines). All sputter yield curves were computed for a surface temperature of 125 K. (For interpretation of the references to color in this figure legend, the reader is referred to the web version of this article.)

this analysis we used the spectral shape and spectral parameters given by Eq. (1) and Table 1 (E6 encounter) in Mauk et al. (2004). The shape of the electron energy spectrum in the energy range 10 keV to 10 MeV was presented by Paranicas et al. (2001). The problem with the used mathematical formulation, though, is that the energy spectrum would steadily increase with decreasing energy if extrapolated to energies below their measurements. Integrating over the complete energy range would thus result in an infinitely large energy flux, which is physically impossible. We thus decided to fit the measurements presented in Fig. 1 of Paranicas et al. (2001) with a kappa function, as was already done for the energetic ions. Fig. 1 contains both the equation presented by Paranicas et al. (2001) (dotted, black line) and the fitted kappa function (solid, black line).

3.3. Sputter yields

Since Europa's icy surface is under constant bombardment by cold and hot plasma ions and electrons, chemical reactions continuously occur within the top layers of the ice. In our model, we assume that the water radiolysis species are sputtered stoichiometrically with respect to their abundance within the surface ice. In the following two subsections we separately describe our implementation of the sputter yields associated with ion bombardment and of the sputter yields associated with electron bombardment.

Table 2
Ice surface composition resulting from radiolysis.

Species	H	H_2	O	O_2	O_3	OH	H_2O	HO_2	H_2O_2
Surface fraction	0.01	0.20	0.01	0.10	0.01	0.01	0.66	0.001	0.001

Table 3
Molecular reaction rates for O_2 and H_2.

Process	Reaction	Cross section (10^{-16}cm^2)	100% flux (cm^{-2}s^{-1})	20% flux (cm^{-2}s^{-1})	Rate 100% flux (10^{-6} s^{-1})	Rate 20% flux (10^{-6} s^{-1})
Photo-dissociation	$O_2 + h\nu \rightarrow O + O$				0.15	0.15
Electron-dissociation	$O_2 + e^- \rightarrow O + O$	0.60	$J_{e^-} = 4.0e10$	$J_{e^-} = 8.0e9$	2.40	0.48
Photo-ionization	$O_2 + h\nu \rightarrow O_2^+ + e^-$				0.02	0.02
Electron-ionization	$O_2 + e^- \rightarrow O_2^+ + 2e^-$	0.60	$J_{e^-} = 4.0e10$	$J_{e^-} = 8.0e9$	2.40	0.48
H^+ charge exchange	$O_2 + H^+ \rightarrow O_2^+ + H$	15	$J_{H^+} = 3.6e8$	$J_{H^+} = 7.3e7$	0.54	0.11
O^+ charge exchange	$O_2 + O^+ \rightarrow O_2^+ + O$	13	$J_{O^+} = 5.7e8$	$J_{O^+} = 1.1e8$	0.74	0.15
S^{++} charge exchange	$O_2 + S^{++} \rightarrow O_2^+ + S^+$	15	$J_{S^{++}} = 3.1e8$	$J_{S^{++}} = 6.2e7$	0.47	0.09
H_2^+ charge exchange	$O_2 + H_2^+ \rightarrow O_2^+ + H_2$	0.8	$J_{H_2^+} = 1e6$	$J_{H_2^+} = 1e6$	1e−4	1e−4
O_2^+ charge exchange	$O_2 + O_2^+ \rightarrow O_2^+ + O_2$	14	$J_{O_2^+} = 1e8$	$J_{O_2^+} = 1e8$	0.14	0.14
Photo-dissociation	$H_2 + h\nu \rightarrow H + H$				0.003	0.003
Electron-dissociation	$H_2 + e^- \rightarrow H + H$	0.42	$J_{e^-} = 4.0e10$	$J_{e^-} = 8.0e9$	1.68	0.34
Photo-ionization	$H_2 + h\nu \rightarrow H_2^+ + e^-$				0.002	0.002
Electron-ionization	$H_2 + e^- \rightarrow H_2^+ + 2e^-$	0.45	$J_{e^-} = 4.0e10$	$J_{e^-} = 8.0e9$	1.80	0.36
H^+ charge exchange	$H_2 + H^+ \rightarrow H_2^+ + H$	2	$J_{H^+} = 3.6e8$	$J_{H^+} = 7.3e7$	0.07	0.01
O^+ charge exchange	$H_2 + O^+ \rightarrow H_2^+ + O$	4.5	$J_{O^+} = 5.7e8$	$J_{O^+} = 1.1e8$	0.26	0.05
S^{++} charge exchange	$H_2 + S^{++} \rightarrow H_2^+ + S^+$	4.5	$J_{S^{++}} = 3.1e8$	$J_{S^{++}} = 6.2e7$	0.14	0.03
H_2^+ charge exchange	$H_2 + H_2^+ \rightarrow H_2^+ + H_2$	7.9	$J_{H_2^+} = 1e6$	$J_{H_2^+} = 1e6$	0.001	0.001
O_2^+ charge exchange	$H_2 + O_2^+ \rightarrow H_2^+ + O_2$	10	$J_{O_2^+} = 1e8$	$J_{O_2^+} = 1e8$	0.10	0.10

3.3.1. Sputtering by ions

Much work has been done to determine water-ice sputter yields during ion bombardment since the very first experiments in the early1980ʼs. These measurements have shown that the absolute sputter yield for impacting ions depends on the mass of the target particle, the mass and the energy of the impactor, the angle of incidence, and the surface temperature (Betz and Wehner, 1983). For the absolute sputter yields of water ice we used the equations presented in Famá et al. (2008) and Johnson et al. (2009), which are the most commonly used water ice sputter yield equations to date. These equations distinguish between two regimes, one where nuclear stopping dominates, and one where electronic stopping dominates. In the nuclear stopping regime (at smaller energies) the momentum of the impactor is passed on to the target particle, whereas in the electronic stopping regime (at higher energies) electrons are responsible for the excitation. A depiction of the energy dependent water-ice sputter yields for impinging H, O, and S ions are shown in Fig. 1, bottom row.

In addition to water molecules, sputtering by ions also releases water radiolysis products, with the same stoichiometric abundance as they are present in the water ice. For our model we compiled water ice radiolysis related data presented in Bar-Nun et al. (1985), Noll et al. (1997), Carlson (1999), Bahr et al. (2001), Spencer and Calvin (2002), Baragiolla (2003), Teolis et al., Zheng et al. (2006), Shi et al. (2011) and Teolis et al. (2017), and implemented their relative abundances as presented in Table 2. These values agree well with sputter yields used by other modelers, e.g. Plainaki et al. (2012) and Cassidy et al. (2013). One caution to mention here, is that whereas the ice sputter yields of H_2O, H_2, and O_2 have been well established, the ice sputter yields of H, O, OH, HO_2 and O_3 are small and largely unknown.

3.3.2. Sputtering by electrons

Water–ice sputter yields for irradiation with electrons were recently presented by Galli et al. (2017). These measurements showed that most particles are released from the water ice as H_2 and O_2 molecules, with an observed ratio of 2:1. In addition, ∼0.3% of the sputtered particles are H_2O_2 molecules. No sputtered H, O, OH, H_2O, HO_2, or O_3 was discernible in the recorded mass spectra. With the H_2, O_2, and H_2O_2 values presented in Table 2 also fulfilling the electron sputter conditions, the same abundance ratios were used when simulating electron sputtering, while all other values were set to 0.

For the absolute sputter yields we used the analytic equation determined by Teolis et al. (2017). Contrary to said equation, though, the measured sputter yields by Galli et al. (2017) did not decrease with energy for energies higher than a few hundred eV, but remained constant at $Y_{O_2} = 2$. We thus modified the Teolis et al. (2017) equation to level out at $Y_{O_2} = 2$ at ∼300 eV. The water equivalent sputter yield (i.e., twice the O_2 sputter yield) of the equation presented by Teolis et al. (2017) and of the measurements presented by Galli et al. (2017) are also shown in the bottom row of Fig. 1.

3.4. Particle ionization and dissociation

Besides escape and return, neutral particles can be removed from the neutral atmosphere through ionization and through dissociation (which results in two dissociation products being added to the neutral atmosphere). There are several particle populations that can lead to ionization of neutral particles in Europa's exosphere. For ionization to be effective these particles need to be within a certain energy range (usually a few ten to hundred eV), though, and we thus accordingly only consider solar photons, cold plasma electrons, cold plasma ions, and ionospheric H_2^+ and O_2^+ when modeling ionization. Additionally, photons and cold plasma electrons can lead to the dissociation of molecules. Table 3 presents all ionization and dissociation processes considered in our Europa model, in the top part for atmospheric O_2 molecules, and in the bottom part for atmospheric H_2 molecules. For photo-dissociation and photo-ionization we use published rates by Huebner et al. (1992) and from http://phidrates.space.swri.edu given for a solar photon flux at 1 AU, and scale them to Europa's distance to the Sun. To determine the electron- and ion-ionization rates, we multiply the effective flux (which includes the particles' temperature) with the interaction specific cross section. The cross sections presented in Table 3 were assembled from Garrett et al. (1985), Tawara et al. (1990), Kanik et al. (1993), Deutsch et al. (2000), Riahi et al. (2006), Straub et al. (1996) and McConkey et al. (2008). For the ionosphere we estimate the O_2 ion

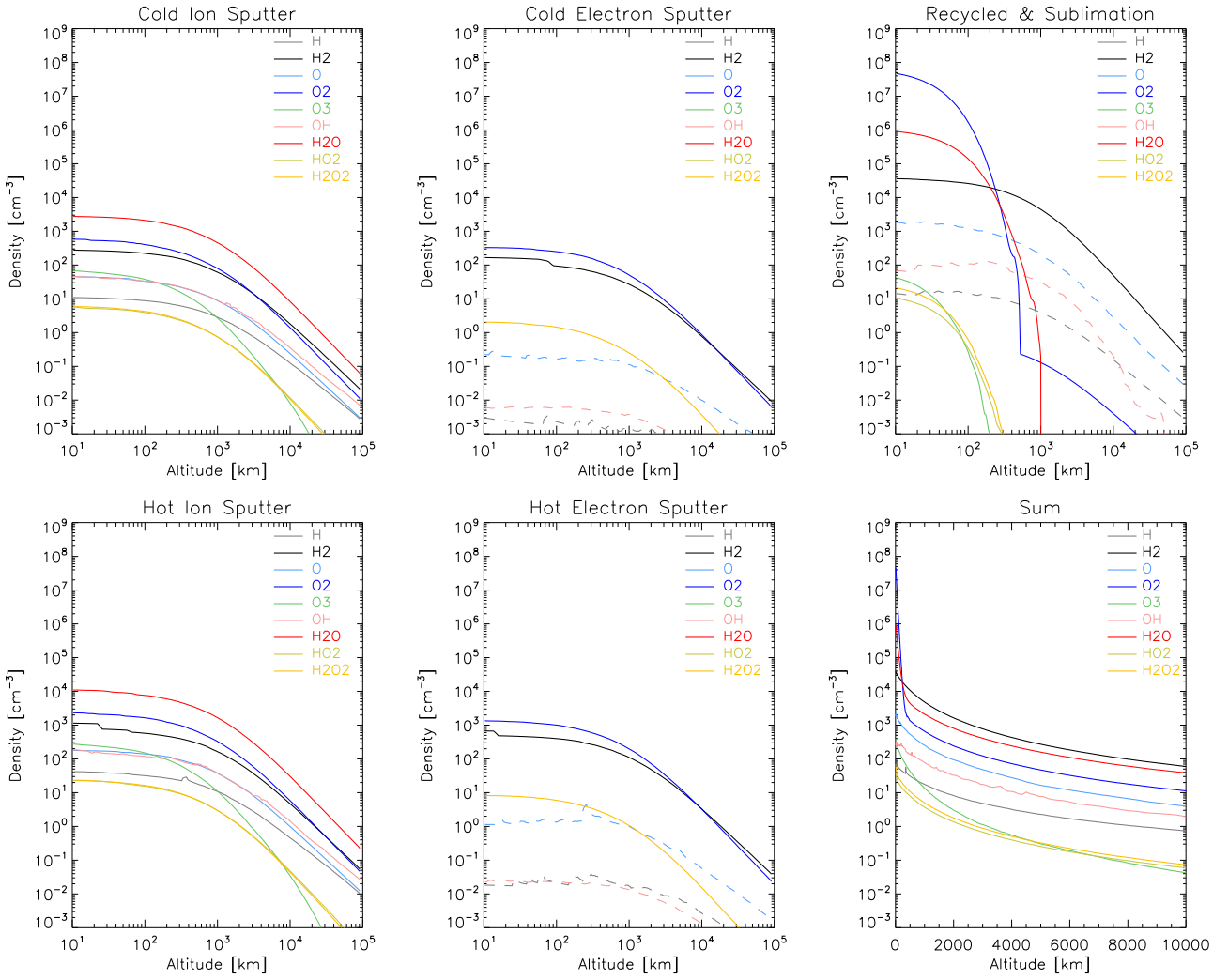

Fig. 2. Simulated density profiles. Solid lines denote species that are directly released from the ice surface, whereas dashed lines denote species that are only present as fragments. The bottom, right plot shows the sum of all processes (note the linear *x*-axis).

flux from the O_2 column density and the O_2 ionization rates, and get $f_{O_2^+} \sim 1 \cdot 10^{12}$ m^{-2}s^{-1},. This agrees well with the ionospheric flux given by Sittler and Strobel (1987) of $f_{O_2^+} < 3 \cdot 10^{12}$ m^{-2}s^{-1} and with the ionospheric flux given by Rubin et al. (2015) of $f_{O_2^+} \sim 1 \cdot 10^{12}$ m^{-2}s^{-1}. With the thermal speed of the O_2 ions we obtain an O_2^+ density of about 4000 cm^{-3} at the surface, which is well within the range of observed ionospheric densities (McGrath et al., 2009).

Similarly, for the H_2 ionosphere, we estimate the H_2 ion flux from the H_2 column density and the H_2 ionization rates, and get $f_{H_2^+} \sim 1 \cdot 10^{10}$ m^{-2}s^{-1}. For comparison with other modeling results in the literature, we show in Table 3 the reactions rates for a cold plasma flux of 100%, and the reaction rates for a cold plasma flux reduced to 20% (used herein). For the water radiolysis products not shown in Table 3, we compute electron reaction rates for a cold electron flux reduced to 20%, and multiply them with a factor of 1.5 to account for all other ionization contributions.

4. Results

For this study, we simulated the release of 10^5 particles per surface ice species (H, H_2, O, O_2, O_3, OH, H_2O, HO_2, and H_2O_2), per plasma type (cold and hot), and per electron and ion type (e^-, H^+, O^{n+}, S^{n+}). The surface temperature was set to 125 K, Europa's mean dayside surface temperature as determined from Spencer et al. (1999). The angle of plasma incidence was taken to be 90° (sub-plasma point). In the calculations performed for this study, step sizes vary from ~300 m at the exobase to ~3,000 km close to the Hill radius.

The resulting density profiles are shown in Fig. 2. The top, left panel shows the exospheric density profiles associated with the cold plasma ions, whereas the bottom, left panel shows the exospheric density profiles associated with the hot plasma ions. The contributions of the three ion types (H^+, O^{n+}, and S^{n+}) are summed up to one curve in each plot. The electron sputter contributions are shown in the center panels, with the top panel showing the contribution from the cold electrons and the bottom panel showing the contribution from the hot electrons. Note that as determined by Galli et al. (2017), only H_2, O_2, and H_2O_2 molecules are directly liberated during electron sputtering. The O, H, and OH density profiles in the electron sputter plots result from fragmentation of H_2, O_2, and H_2O_2 induced by photons and electrons within the exosphere.

In addition, at a given ice surface temperature, for some species the vapor pressure is high enough for sublimation to occur. In this study, we assume that all molecules generated through radiolysis are formed below the surface and are trapped within the water ice. Thus, the radiolysis products sublimate with the water molecules,

except for O, H, and OH, the recombination rates of which are too high for the sublimation rates to be effective. We show the sublimation density profiles for H_2, O_2, O_3, H_2O, HO_2, and H_2O_2 in the top right panel of Fig. 2.

Since H_2 and O_2 do not freeze out on the surface of Europa, their density in the atmosphere increases, until a balance between the returning neutral flux and the atmospheric loss via neutral escape, ionization, and fragmentation is reached. These non-sticking particles interact with the surface repeatedly, whereby they are quickly thermalized to the surface temperature. For the non-sticking particles we thus model an additional atmospheric source (termed recycled particles), where the source flux from the surface is equal to the returning fraction of the sputtered and sublimated neutral flux divided by the loss rate (ionization, fragmentation, and escape). Since the particles are thermalized to the local surface temperature, we again model a population with an energy spectrum represented by a Maxwellian distribution around 125 K. The density profiles resulting from 1 million modeled particles per species is also shown in the top right panel of Fig. 2. Note again, that only H_2, and O_2 were directly released from the surface; the H and the O density profiles belong to fragments born in the exosphere.

As a summary, the sum of all atmospheric sources is shown in the bottom right panel of Fig. 2 (note that the x-axis is linear in this panel). Complementing this plot, the exobase number densities and column density values for each surface species and source process are listed in Table 4.

As mentioned in the previous section, each exospheric particle meets one of the following fates: (i) escape, (ii) return, (iii) ionization, or (iv) fragmentation. Knowing the surface sputtered and surface sublimated release flux, as well as the fraction of escaping and ionized particles, one can compute the global neutral and the global ion escape rate. Since the fate of a newly ionized particle cannot be determined in our model, we assume that half of the generated ions return to the surface, whereas the other half escapes from Europa's atmosphere. The sputtered and sublimated/recycled surface fluxes computed by our simulations are listed in Table 5. To compute the global neutral and ion escape rates we multiply the sputtered fluxes with the area of the sub-plasma hemisphere in the case of cold plasma sputtering, and with Europa's complete surface area in the case of hot plasma sputtering. In addition, we multiply the cold plasma result with $\cos(30°)$, the cosine of the average plasma impact angle. For the sublimated species, we assume that particles only sublimate from the dayside hemisphere. Since our simulations already use a surface temperature of 125 K (the average dayside surface temperature), no further averaging is necessary, and we can directly multiply our results with the area of the dayside hemisphere. The resulting global neutral and ion escape rates are presented in Table 6.

Having determined that Europa's atmosphere is dominated by an O_2 atmosphere close to the surface, we can estimate the amount of collisions among the O_2 molecules to check if our assumption of a collision-less exosphere is valid. From the van der Waals radius of O_2 of 152 pm we get a geometrical cross section of $\sigma_{O_2} = 7.26 \cdot 10^{-16}$ cm^2, which we use for the collisions of thermal oxygen molecules. With an O_2 surface density of $N0(O_2) = 7{\cdot}10^7$ cm^{-3} we get a mean free path of $\lambda_{O_2} = 197$ km. Thus, even at Europa's surface, the mean free path of the oxygen molecules is much larger than the O_2 scale height of 27 km and the probability of an O_2–O_2 collision in the exosphere is about $p_{\mathrm{coll}} \approx 1 - \exp(-NC \cdot \sigma) = 12\%$. The approximation of a collision-free exosphere starting at the surface is thus justified.

A second check we performed was to determine whether the remaining 20% of cold plasma that is not deflected around Europa by the electro-magnetic field can in fact reach Europa's surface unhindered. For the passage of the O ions through the O_2 atmosphere

Table 4
Surface densities (N0) and radial column densities (NC) listed separately for each surface release process.

Species	Cold ion sputtered		Hot ion sputtered		Cold electron sputtered		Hot electron sputtered		Recycled sputtered		Sublimated		Total	
	N0 (cm^{-3})	NC (cm^{-2})	N0 (cm^{-3})	NC (cm^{-2})	N0 (cm^{-3})	NC (cm^{-2})	N0 (cm^{-3})	NC (cm^{-2})	N0 (cm^{-3})	NC (cm^{-2})	N0 (cm^{-3})	NC (cm^{-2})	N0 (cm^{-3})	NC (cm^{-2})
H	1.14E+01	1.17E+09	4.34E+01	4.41E+09	4.01E-03	1.37E+06	1.87E-02	1.31E+07	4.43E+00	3.44E+08	1.40E+01	1.29E+09	7.33E+01	7.22E+09
H_2	9.49E+02	2.37E+10	1.21E+03	6.32E+10	1.77E+02	1.05E+10	6.87E+02	4.26E+10	3.81E+04	1.73E+12	1.50E+03	6.11E+10	4.26E+04	1.93E+12
O	2.72E+01	3.39E+09	1.72E+02	1.42E+10	4.63E−01	5.70E+07	1.19E+00	4.18E+08	1.70E+03	8.55E+10	7.25E-01	2.79E+07	1.91E+03	1.04E+11
O_2	6.26E+02	3.11E+10	2.61E+03	1.27E+11	3.38E+02	1.97E+10	1.26E+03	7.63E+10	7.00E+07	1.75E+14	3.11E+03	7.78E+09	7.00E+07	1.75E+14
O_3	1.11E+02	1.60E+09	2.50E+02	6.45E+09							7.50E+01	1.22E+08	4.35E+02	8.18E+09
OH	5.07E+01	3.80E+09	1.94E+02	1.49E+10	8.48E−03	1.77E+06	3.43E−02	7.10E+06			7.89E+01	1.03E+10	3.24E+02	2.91E+10
H_2O	2.77E+03	1.74E+11	1.22E+04	6.31E+11							1.11E+06	5.21E+12	1.12E+06	6.02E+12
HO_2	5.35E+00	2.93E+08	2.51E+01	1.17E+09							1.25E+01	3.82E+07	4.29E+01	1.50E+09
H_2O_2	5.92E+00	2.97E+08	2.24E+01	1.18E+09	1.75E+00	1.00E+08	6.37E+00	4.21E+08			3.16E+01	7.45E+07	6.80E+01	2.07E+09

Table 5
Surface fluxes listed for each surface release process separately.

Species	$F_{cold\ ion\ sputtered}$ ($cm^{-2}s^{-1}$)	$F_{hot\ ion\ sputtered}$ ($cm^{-2}s^{-1}$)	$F_{cold\ electron\ sputtered}$ ($cm^{-2}s^{-1}$)	$F_{hot\ electron\ sputtered}$ ($cm^{-2}s^{-1}$)	$F_{recycled\ sputtered}$ ($cm^{-2}s^{-1}$)	$F_{sublimated}$ ($cm^{-2}s^{-1}$)	F_{total} ($cm^{-2}s^{-1}$)
H	1.15E+07	4.97E+07	–	–	–	–	6.12E+07
H_2	2.35E+08	1.01E+09	1.49E+08	5.99E+08	4.36E+09	1.65E+08	6.52E+09
O	1.15E+07	4.97E+07	–	–	–	–	6.12E+07
O_2	1.17E+08	5.06E+08	7.44E+07	3.00E+08	1.87E+12	8.27E+07	1.87E+12
O_3	1.15E+07	4.98E+07	–	–	–	1.65E+06	6.30E+07
OH	1.15E+07	4.97E+07	–	–	–	–	6.12E+07
H_2O	7.57E+08	3.27E+09	–	–	–	4.11E+10	4.51E+10
HO_2	1.16E+06	5.02E+06	–	–	–	4.13E+05	6.59E+06
H_2O_2	1.17E+06	5.06E+06	4.46E+05	1.80E+06	–	8.27E+05	9.31E+06

Table 6
Global neutral and ion escape rates.

Species	$Q_{neutral}$ (s^{-1})	Q_{ion} (s^{-1})
H	6.61E+25	2.95E+24
H_2	5.46E+26	1.57E+25
O	3.02E+25	2.75E+25
O_2	9.12E+25	9.65E+25
O_3	8.04E+22	1.25E+23
OH	4.20E+25	5.35E+24
H_2O	4.90E+26	5.52E+25
HO_2	4.71E+23	8.78E+22
H_2O_2	5.61E+23	1.03E+23

we consider two cross sections for the O–O_2 collision. First we assume that a collision occurs when the distance between the center of the two reactant particles is less than the sum of their radii (Atkins, 2000), which yields $\sigma_{O_2-O} = 3.62 \times 10^{-16}$ cm^2. For the second check we apply a collision cross section of $\sigma \approx 1 \times 10^{-15}$ cm^{-2}, a value commonly used for a variety of collisions, which also approximates the value for O–O collisions (Tully and Johnson, 2001). Using these cross sections we get mean free paths for the O ions in the O_2 atmosphere of 395 km and 143 km, and collision probabilities between 6% and 16% for O^+–O_2 collisions. Since the mean free path of the ions is larger than the O_2 scale height, the flux of magnetospheric ions will hardly be attenuated when passing through the exosphere before they hit the surface.

To better quantify the interaction probability of magnetospheric ions passing through an O_2 exosphere we additionally performed SRIM calculations (http://www.SRIM.org), where we simulated the passage of O^+ ions with an energy of 479 eV through an O_2 atmosphere with a column density of $NC(O_2) = 1.75 \cdot 10^{14}$ cm^{-2}. The resulting 99.9% transmission, the less than 2% energy loss, and the less than 5% collision probability agree well with our computations above, and confirm our assumption that the cold plasma that is not deflected around Europa reaches the surface almost unhindered. In addition, the SRIM calculations show that sputtering of atmospheric particles by magnetospheric ions has a sputter yield of less than 1%, and that almost no ions ($\leq 3 \cdot 10^{-4}$) are backscattered from the atmosphere as energetic neutral atoms.

5. Discussion

5.1. Comparison to observational data and previously published models

Table 7 compares our results to available observations and results from previously published models. In general, our results agree well with observational values and previously published model values, with the notable difference that our results are based on first principles and are not scaled to fluxes or densities of observed data. As in many previously published models, our calculations result in a bound thermalized O_2 atmosphere with an extended corona of light H_2 molecules. The origin of the exosphere is sputtering by cold and hot ions, to about equal amounts. Additionally, electrons are an important contributor for O_2 and H_2.

Whereas our modeled O_2 surface particle and column densities agree very well with previously published values, our atomic O content (which mainly comes from dissociated O_2) is somewhat lower than the 2005 observation, while it is in agreement with the 1995 and 1998 observations (from which only 3 σ upper limits could be determined) and previously published model results. There are several possibilities for the discrepancy between the observational values published by Hansen et al. (2005) and the values resulting from modeling: (1) the oxygen emission model used by Hansen et al. (2005) is inaccurate, which leads to inaccuracies in the determined O content, (2) O_2 dissociation was exceptionally effective during the 2005 observation, i.e., the electron flux responsible for the O_2 dissociation was much higher than on average, or (3) the modelers in general underestimate the O_2 electron dissociation rate. Without any further observational data, it is impossible to say which of these three assumptions (or combination thereof) is valid. It is also noteworthy, that in our model the electron flux, which is the main dissociation agent, has been drastically reduced based on plasma modeling results (Sittler and Strobel, 1987; Rubin et al., 2015). If we had assumed zero plasma deflection around Europa, our O surface density would increase by at least a factor of 5, and would accordingly agree much better with previously published surface density values. Finally, note that there is a 'tail' in the O_2 curve that starts at approximately 600 km. This 'tail' is a result of the dissociation of O_3 molecules, which contain quite a high dissociation energy.

While our calculated H_2 surface density and column density also agree well with previously published data, again, the resulting dissociation product, H is lower by almost two an orders of magnitude than the observational value. Another source for H is dissociation of H_2O. In our model, we simulated profiles for an average dayside surface temperature of 125 K, which gives a low water sublimation flux, whereas the observations are on the sun-illuminated side, where the average surface

No observational data exists for atmospheric OH or H_2O (except for a plume observation), but again, our modeled surface density and column densities agree very well with previously published modeling data.

5.2. Cold and hot plasma contribution

In general, sputter yields of water ice increases dramatically for higher energies (see Fig. 1), therefore, the hot plasma population, although of much lower density than the thermal plasma, contributes significantly to the total sputter yield. Concerning the different ion types, for the cold plasma the largest sputter contributor are the O ions (57.47%), followed by the S ions (40.42%) and only a minor part of the sputtered flux is attributed to the H ions (2.11%). For the hot plasma, the contribution by the three ion types

Table 7
Comparison between observations, previously published models, and the results published herein. Note that all observations were accomplished through spectroscopy, i.e., column densities (NC) were obtained through calibration and surface densities (N0) were obtained through modeling.

Species	N0 (cm^{-3})	NC (cm^{-2})	Method	Instrument	Comment	Ref.
O	–	**<2e14**	**Observed**	**HST/GHRS**	–	Hall et al. (1995)
	–	**<2.3e14**	**Observed**	**HST/GHRS**	–	Hall et al. (1998)
	–	**<3.4e14**	**Observed**	**HST/GHRS**	–	Hall et al. (1998)
	–	**<1.6e14**	**Observed**	**HST/GHRS**	–	Hall et al. (1998)
	(8.5–15)e5	**(1.7–3.1)e13**	**Observed**	**Cassini/UVIS**	**Extended (7 R_E) component**	Hansen et al. (2005)
	–	(0.09–260)e12	Modeled		See paper for different scenarios	Shematovich et al. (2005)
	–	(3.8–4.2)e12	Modeled		See paper for different scenarios	Shematovich et al. (2005)
	–	1.2e12	Modeled		Sputter; day–night average	Smyth and Marconi (2006)
	1.91e3	1.04e11	Modeled		Sub-plasma point	This work
O_2	–	**1.5e15**	**Inferred**	**HST / GHRS**	–	Hall et al. (1995)
	–	**(2.4–12)e14**	**Inferred**	**HST / GHRS**	**Scale height 20–300 km**	Hall et al. (1998)
	–	**(3.7–14)e14**	**Inferred**	**HST / GHRS**	**Scale height 20–300 km**	Hall et al. (1998)
	–	**(3.5–11)e14**	**Inferred**	**HST / GHRS**	**Scale height 20–300 km**	Hall et al. (1998)
	(3.7–6.2)e7	**(7.4–12.4)e14**	**Inferred**	**Cassini / UVIS**	**Scale height ∼200 km**	Hansen et al. (2005)
	–	**> 6e14**	**Inferred**	**ACS / UV**	–	Saur et al. (2011)
	–	**(3–6)e14**	**Inferred**	**HST / STIS**	–	Roth et al. (2016)
	1e3	1e11	Modeled		Sputtered O_2 with scale height ∼200 km	Ip et al. (1998)
	(1–19)e8	–	Modeled		Thermal O_2 with scale height ∼20 km	Ip et al. (1998)
	–	5e14	Modeled		Sputtered O_2 with scale height ∼145 km	Saur et al. (1998)
	1e8	–	Modeled		Sputtered O_2 with scale height ∼100 km	Johnson et al. (1998)
	–	(0.9–13)e15	Modeled		See paper for different scenarios	Shematovich et al. (2005)
	–	(7.8–9.9)e14	Modeled		See paper for different scenarios	Shematovich et al. (2005)
	–	4.4e14	Modeled		Sputter; day-night average	Smyth and Marconi (2006)
	1e8	1e15	Modeled		Assumed background atmosphere	Leblanc et al. (2005)
	(1.5–3.3)e7	(3–15)e14	Modeled		Subpolar hemisphere and anti-subsolar hemisphere	Plainaki et al. (2012)
	–	(1.5–4.6)e15	Modeled		Sputter at different orbital configurations	Plainaki et al. (2013)
	∼1e7	1.58e14	Modeled		Global average and day-side equator, respectively	Teolis et al. (2017)
	7.00e7	1.75e14	Modeled		Sub-plasma point	This work
OH	–	(1.4–5.5)e10	Modeled		See paper for different scenarios	Shematovich et al. (2005)
	–	1.9e11	Modeled		Sputter; day–night average	Smyth and Marconi (2006)
	3.42e2	2.91e10	Modeled		Sub-plasma point	This work
H_2	–	7.7e13	Modeled		Sputter; day–night average	Smyth and Marconi (2006)
	(4.0–14)e4	–	Modeled		Subpolar hemisphere and anti-subsolar hemisphere	Plainaki et al. (2012)
	∼1e6	2.51e13	Modeled		Global average and day-side equator, respectively	Teolis et al. (2017)
	4.26e4	1.93e12	Modeled		Sub-plasma point	This work
H	**(1.5–2.25)e3**	–	**Observed**	**HST / STIS**	**intrinsic variability observed**	Roth et al. (2017)
	–	7.6e10	Modeled		Sputter; day–night average	Smyth and Marconi (2006)
	7.33e1	7.22e9	Modeled		Sub-plasma point	This work
H_2O	–	**1.5e16**	**Inferred**	**HST / STIS**	**plume with scale height 200 ± 100 km**	Roth et al. (2014)
	–	(9.2–87)e11	Modeled		See paper for different scenarios	Shematovich et al. (2005)
	–	2.30e12	Modeled		Sputter; day–night average	Smyth and Marconi (2006)
	2.7e4		Modeled		Sputter	Plainaki et al. (2010)
	1.5e5	–	Modeled		Average over both hemispheres	Plainaki et al. (2012)
	∼1e5	7.94e14	Modeled		Global average and day-side equator, respectively	Teolis et al. (2017)
	1.12e6	6.02e12	Modeled		Sub-plasma point	This work

is even more imbalanced, with H contributing only 0.15%, O contributing 16.09% and S contributing 83.76% to the overall sputtered flux.

The sputter yield of electrons is high already at low electron energies. Thus, even though the cold electrons have a low mean energy related to their average movement with the co-rotation velocity, their temperature of ∼20 eV is sufficient for a substantial sputter contribution to the exosphere. In fact, electrons and ions contribute almost equally to the overall sputter flux, with an electron to ion sputtered flux ratio of 0.6:1 for both H_2 and O_2 and 0.4:1 for H_2O_2. Given the discrepancy between the sputter yields for electrons in the literature (Teolis et al., 2017; Galli et al., 2017), our calculation of the hot electron contribution to the exosphere might be over-estimated. Since the contribution by hot electrons to sputtering is almost an order of magnitude smaller than the contribution by cold electrons, though, this does not significantly affect the overall density profiles, and we judge our approach as justified. In addition, surface charging can limit the flux of cold ions reaching Europa's surface. Having already accounted for a cold plasma electron diversion of 20%, though, and considering the uncertainty associated with this diversion rate, we are confident that this value appropriately represents all significant reduction contributions.

5.3. Ion and neutral particle escape

Table 6 shows that the global neutral escape rate is dominated by the light H_2 molecules, which escape Europa's gravity to form Europa's torus. Other species with high neutral escape rates include the abundant but heavier molecules H_2O and O_2. Global ion escape rates are dominated by sputtered O_2, H_2O, O, and H_2, with most ions generated by electron-impact-ionization (cf. Table 3). Over time, the escaping exospheric particles will become part of Jupiter's magnetospheric plasma. This again results in (1) mass loading of the magnetospheric plasma by ion pick-up, (2) induced currents in the ionosphere (if present), and in (3) the pile-up of the magnetospheric magnetic field in front of Europa. These plasma-surface and plasma-exosphere interaction processes will all occur near the moon, at lengths scales commensurate with the scale height of the dominant exospheric species, thermal O_2, and will result in a reduction of the magnetospheric plasma reaching the surface.

6. Conclusion

In summary, the most important findings of our calculations are as follows:

- Europa's atmosphere is dominated near the surface (<a few 100 km) by a bound, recycled O_2 atmosphere with a column density of $N_C(O_2)$ $\sim 2{\cdot}10^{14}$ cm^{-2} and is sustained by a surface source rate of $\sim 2{\cdot}10^{12}$ cm^{-2} s^{-1}
- Further out (> few 100 km), Europa's atmosphere is dominated by an extended corona of recycled, light H_2 molecules with a column density of $N_C(H_2)$ $\sim 2{\cdot}10^{12}$ cm^{-2} and a supply rate of $\sim 7{\cdot}10^{9}$ cm^{-2} s^{-1}
- The hot and cold plasma populations contribute about equally to the overall sputtered flux, with a flux ratio of 1:4.3
- Both ions and electrons play an important role in the generation of Europa's ice sputtered atmosphere, with surface flux ratios of 1:0.4–0.6
- Magnetospheric S ions are by far the most important sputter agents (inducing 76% of the sputtered flux), followed by O (24%), and with only a minor contribution by H (0.5%)
- H_2 dominates the global neutral escape rate ($5.46{\cdot}10^{26}$ s^{-1}), followed by H_2O ($4.90{\cdot}10^{26}$ s^{-1}), and O_2 ($9.12{\cdot}10^{25}$ s^{-1})
- The global ion escape rate is dominated by O_2 ($9.65{\cdot}10^{25}$ s^{-1}), followed by H_2O ($5.52{\cdot}10^{25}$ s^{-1}), O ($2.75{\cdot}10^{25}$ s^{-1}), and H_2 ($1.57{\cdot}10^{25}$ s^{-1})

All atmospheric observations to date were obtained from remote sensing spectroscopy, i.e., the observed quantity is the line-of-sight brightnesses of optical transitions, which had to be converted to column densities through calibration, and in a second step to surface densities by making certain assumptions (e.g. on atmospheric density profiles or electron impact excitation rates) or by using exospheric models. No direct measurements, i.e., in situ measurements of Europa's exosphere, are available so far.

This will change with the upcoming JUpiter ICy moons Explorer (JUICE) mission (Grasset et al., 2013), though, a mission which is currently in implementation by the European Space Agency (ESA). JUICE will investigate Europa, Callisto and Ganymede, with particular emphasis on Ganymede. Among the planned scientific investigations of JUICE are explorations of the chemical composition of the Galilean moons and of their exospheres. The Particle Environment Package (PEP) suite, one of the scientific payloads of JUICE, contains instruments for the comprehensive measurements of electrons, ions and neutrals in the Galilean moons' vicinity (Barabash et al., 2013). The Neutral and Ion Mass spectrometer (NIM), which is part of the PEP instrument suite, will measure the neutral and ion composition of Europa's exosphere during two dedicated flybys (Wurz et al., 2014). In addition to the NIM measurements, the ion and electron instruments of the PEP suite will fully characterize the plasma and energetic particle environment at Europa. Moreover, there are several other instrument on JUICE that will be performing exospheric measurements, along with other science objectives, which are MAJIS (Langevin et al., 2013), SWI (Hartogh et al., 2013), UVS (Gladstone et al., 2013), and RPWI (Wahlund and the JUICE-RPWI team, 2013).

References

Atkins, P., 2000. Physical Chemistry: Sixth Edition. Freeman and Company, New York, pp. 29–30.

Bagenal, F., Sidrow, E., Wilson, R.J., Cassidy, T.A., Dols, V., Crary, F.J., Steffl, A.J., Delamere, P.A., Kurth, W.S., Paterson, W.R., 2015. Plasma conditions at Europa's orbit. Icarus 261, 1–13. doi:10.1016/j.icarus.2015.07.036.

Bahr, D.A., Famá, M., Vidal, R.A., Baragiola, R.A., 2001. Radiolysis of water ice in the outer solar system: sputtering and trapping of radiation products. J. Geophys. Res. 106, 33285–33290. doi:10.1029/2000JE001324.

Bar-Nun, A., Herman, G., Rappaport, M.L., Mekler, Y., 1985. Sputtering of water ice at 30–140 K by 0.5–6.0 keV H(+) and Ne(+) ions. In: Klinger, J., Benest, D., Dollfus, A., Smoluchowski, R. (Eds.), NATO Advanced Science Institutes (ASI) Series C. In: NATO Advanced Science Institutes (ASI) Series C, 156, pp. 287–298.

Barabash, S., Wurz, P., Brandt, P., Wieser, M., Holmström, M., Futaana, Y., Stenberg, G., Nilsson, H., Eriksson, A., Tulej, M., Vorburger, A., Thomas, N., Paranicas, C., Mitchell, D.G., Ho, G., Mauk, B.H., Haggerty, D., Westlake, J.H., Fränz, M., Krupp, N., Roussos, E., Kallio, E., Schmidt, W., Szego, K., Szalai, S., Khurana, K., Jia, X., Paty, C., Wimmer-Schweingruber, R.F., Heber, B., Kazushi, A., Grande, M., Lammer, H., Zhang, T., McKenna-Lawlor, S., Krimigis, S.M., Sarris, T., Grodent, D., 2013. Particle environment package (PEP). In: Proceedings of the European Planetary Science Congress 2013, 8, p. 709. held 8–13 September, London, UK.

Baragiolla, R.A., 2003. Water ice on outer solar system surfaces: basic properties and radiation effects. Planet. Space Sci. 51, 953–961. doi:10.1016/j.pss.2003.05.007.

Betz, G., Wehner, G.K., 1983. Sputtering of multicomponent materials. In: Behrish, R. (Ed.), Sputtering by Particle Bombardment II. Topics in Applied Physics, 52. Springer, Berlin, Heidelberg.

Carlson, R.W., 1999. A tenuous carbon dioxide atmosphere on Jupiter's moon callisto. Science 283 (820). doi:10.1126/science.283.5403.820.

Cassidy, T.A., Johnson, R.E., 2005. Monte carlo model of sputtering and other ejection processes within a regolith. Icarus 176, 499–507. doi:10.1016/j.icarus.2005.02.013.

Cassidy, T.A., Paranicas, C.P., Shirley, J.H., Dalton III, J.B., Teolis, B.D., Johnson, R.E., Kamp, L., Hendrix, A.R., 2013. Magnetospheric ion sputtering and water ice grain size at Europa. Planet. Space Sci. 77, 64–73. doi:10.1016/j.pss.2012.07.008.

Cooper, J.F., Johnson, R.E., Mauk, B.H., Garrett, H.B., Gehrels, N., 2001. Energetic ion and electron irradiation of the icy galilean satellites. Icarus 149, 133–159. doi:10.1006/icar.2000.6498.

Deutsch, H., Becker, K., Matt, S., Märk, T.D., 2000. Theoretical determination of absolute electron-impact ionization cross sections of molecules. Int J Mass Spectrom 197, 37–69. doi:10.1016/S1387-3806(99)00257-2.

Divine, N., Garrett, H.B., 1983. Charged particle distributions in Jupiter's magnetosphere. J. Geophys. Res. 88, 6889–6903. doi:10.1029/JA088iA09p06889.

Famá, M., Shi, J., Baragiola, R.A., 2008. Sputtering of ice by low-energy ions. Surf. Sci. 602, 156–161. doi:10.1016/j.susc.2007.10.002.

Galli, A., Vorburger, A., Wurz, P., Pommerol, A., Cerubini, R., Jost, B., Poch, O., Tulej, M., Thomas, N., 2017. 0.2 to 10 keV electrons interacting with water ice: Radiolysis, sputtering, and sublimation. Planet. Space Sci. doi:10.1016/j.pss.2017.11.016.

Garrett, B.C., Redmon, L.T., McCurdy, C.W., Redmon, M.J., 1985. Electronic excitation and dissociation of O2 and S2 by electron impact. Phys. Rev. A 32 (6), 3366–3375.

Gladstone, R., Retherford, K., Steffl, A., Eterno, J., Davis, M., Versteeg, M., Greathouse, T., Araujo, M., Walther, B., Persson, K., Persyn, S., Dirks, G., McGrath, M., Feldman, P., Bagenal, F., Spencer, J., Schindhelm, E., Fletcher, L., 2013. The ultraviolet spectrograph (UVS) on ESA's JUICE mission. In: Proceedings of the European Planetary Science Congress 2013, 8, p. 394. held 8–13 September, London, UK.

Grasset, O., Dougherty, M.K., Coustenis, A., Bunce, E.J., Erd, C., Titov, D., Blanc, M., Coates, A., Drossart, P., Fletcher, L.N., Hussmann, H., Jaumann, R., Krupp, N., Lebreton, J.-P., Prieto-Ballesteros, O., Tortora, P., Tosi, F., Hoolst, T.V., 2013. JUpiter ICy Moons explorer (JUICE): an ESA mission to orbit ganymede and to characterise the jupiter system. Planet. Space Sci. 78, 1–21. doi:10.1016/j.pss.2012.12.002.

Hall, D.T., Feldman, P.D., McGrath, M.A., Strobel, D.F., 1998. The far-Ultraviolet oxygen Airglow of Europa and ganymede. Astrophys. J. 499, 475–481. doi:10.1086/305604.

Hall, D.T., Strobel, D.F., Feldman, P.D., McGarth, M.A., Weaver, H.A., 1995. Detection of an oxygen atmosphere on Jupiter's moon Europa. Nature 373, 677–679. doi:10.1038/373677a0.

Hansen, C.J., Shemansky, D.E., Hendrix, A.R., 2005. Cassini UVIS observations of Europa's oxygen atmosphere and torus. Icarus 176, 305–315. doi:10.1016/j.icarus.2005.02.007.

Hartogh, P., Barabash, S., Beaudin, G., Börner, P., Bockeleé-Morvan, D., Boogaerts, W., Cavalié, T., Christensen, U.R., Dannenberg, A., Eriksson, P., Fränz, M., Fouchet, T., Frisk, U., Hocke, K., Janssen, C., Jarchow, C., Kasai, Y., Kikuchi, K., Krieg, J.-M., Krupp, N., Kuroda, T., Lellouch, E., Loose, A., Maestrini, A., Manabe, T., Medvedev, A.S., Mendrok, J., Miettinen, E.P., Moreno, R., Murk, A., Murtagh, D., Nishibori, T., Rengel, M., Rezac, L., Sagawa, H., Steinmetz, E., Thomas, B., Urban, J., Wicht, J., 2013. The submillimetre wave instrument on JUICE. In: Proceedings of the European Planetary Science Congress 2013, 8, p. 710. held 8–13 September, London, UK.

Hodges Jr., R.R., 1994. Monte carlo simulation of the terrestrial hydrogen exosphere. J. Geophys. Res. 99, 23. doi:10.1029/94JA02183.

Huebner, W.F., Keady, J.J., Lyon, S.P., 1992. Solar photo rates for planetary atmospheres and atmospheric pollutants. Astrophys. and Space Sci. 195 (1), 1–294.

Ip, W.-H., Williams, D.J., McEntire, R.W., Mauk, B.H., 1998. Ion sputtering and surface erosion at europa. Geophys. Res. Lett. 25, 829–832. doi:10.1029/98GL00472.

Johnson, R.E., Burger, M.H., Cassidy, T.A., Leblanc, F., Marconi, M., Smyth, W.H., 2009. Composition and Detection of Europas Sputter-induced Atmosphere. University of Arizona Press, Tucson, pp. 507–527.

Johnson, R.E., Killen, R.M., Waite Jr., J.H., Lewis, W.S., 1998. Europa's surface composition and sputter-produced ionosphere. Geophys. Res. Lett. 25, 3257–3260. doi:10.1029/98GL02565.

Joy, S.P., Kivelson, M.G., Walker, R.J., Khurana, K.K., Russell, C.T., Ogino, T., 2002. Probabilistic models of the Jovian magnetopause and bow shock locations. J. Geophys. Res 107, 1309. doi:10.1029/2001JA009146.

Kanik, I., Trajmar, S., Nickel, J.C., 1993. Total electron scattering and electronic state excitations cross sections for O_2, CO, and CH_4. J. Geophys. Res. 98, 7447–7460. doi:10.1029/92JE02811.

Kivelson, M.G., Khurana, K.K., Volwerk, M., 2009. Europa's Interaction with the Jovian Magnetosphere. In: Pappalardo, R.T., McKinnon, W.B., Khurana, K.K. (Eds.), Europa. University of Arizona Press, Tucson, p. 545.

Langevin, Y., Piccioni, G., the MAJIS Team, 2013. MAJIS (Moons and Jupiter imaging spectrometer) for JUICE: objectives for the galilean satellites. in: Proceedings of

the European Planetary Science Congress 2013, held 8–13 September, London, UK 8, 548.
Leblanc, F., Potter, A.E., Killen, R.M., Johnson, R.E., 2005. Origins of Europa Na cloud and torus. Icarus 178, 367–385. doi:10.1016/j.icarus.2005.03.027.
Mauk, B.H., Mitchell, D.G., McEntire, R.W., Paranicas, C.P., Roelof, E.C., Williams, D.J., Krimigis, S.M., Lagg, A., 2004. Energetic ion characteristics and neutral gas interactions in Jupiter's magnetosphere. J. Geophys. Res. (Space Phys.) 109, A09S12. doi:10.1029/2003JA010270.
McConkey, J.W., Malone, C.P., Johnson, P.V., Winstead, C., McKoy, V., Kanik, I., 2008. Electron impact dissociation of oxygen-containing molecules a critical review. Phys. Rep. 466, 1–103. doi:10.1016/j.physrep.2008.05.001.
McGrath, M.A., Hansen, C.J., Hendrix, A.R., 2009. Observations of Europa's Tenuous Atmosphere. In: Pappalardo, R.T., McKinnon, W.B., Khurana, K.K. (Eds.), Europa. Univ. of Arizona Press, Tucson, pp. 485–505.
McGrath, M.A., Lellouch, E., Strobel, D.F., Feldman, P.D., Johnson, R.E., 2004. Satellite atmospheres. In: Bagenal, F., Dowling, T., McKinnon, W.B. (Eds.), Jupiter-The Planet, Satellites & Magnetosphere. Cambridge University Press, Cambridge, pp. 457–483.
Noll, K.S., Roush, T.L., Cruikshank, D.P., Johnson, R.E., Pendleton, Y.J., 1997. Detection of ozone on Saturn's satellites RHEA and dione. Nature 388, 45–47. doi:10.1038/40348.
Paranicas, C., Carlson, R.W., Johnson, R.E., 2001. Electron bombardment of Europa. Geophys. Res. Lett. 28, 673–676. doi:10.1029/2000GL012320.
Paranicas, C., Ratliff, J.M., Mauk, B.H., Cohen, C., Johnson, R.E., 2002. The ion environment near Europa and its role in surface energetics. Geophys. Res. Lett. 29, 18-1–18-4. doi:10.1029/2001GL014127.
Plainaki, C., Milillo, A., Mura, A., Orsini, S., Cassidy, T., 2010. Neutral particle release from Europa's surface. Icarus 210, 385–395. doi:10.1016/j.icarus.2010.06.041.
Plainaki, C., Milillo, A., Mura, A., Orsini, S., Massetti, S., Cassidy, T., 2012. The role of sputtering and radiolysis in the generation of Europa exosphere. Icarus 218, 956–966. doi:10.1016/j.icarus.2012.01.023.
Plainaki, C., Milillo, A., Mura, A., Saur, J., Orsini, S., Massetti, S., 2013. Exospheric o_2 densities at Europa during different orbital phases. Planet. Space Sci. 88, 42–52. doi:10.1016/j.pss.2013.08.011.
Retherford, K.D., Spencer, J.R., Gladstone, G.R., Stern, S.A., Saur, J., Strobel, D.F., Slater, D.C., Steffl, A.J., Parker, J.W., Versteeg, M., Davis, M.W., Throop, H., Young, L.A., 2007. Icy Galilean Satellite UV Observations by New Horizons and HST. AGU. AGU Fall Meeting Abstracts.
Riahi, R., Teulet, P., Ben Lakhdar, Z., Gleizes, A., 2006. Cross-section and rate coefficient calculation for electron impact excitation, ionisation and dissociation of H_2 and OH molecules. Eur. Phys. J. D 40, 223–230. doi:10.1140/epjd/e2006-00159-2.
Roth, L., Retherford, K.D., Ivchenko, N., Schlatter, N., Strobel, D.F., Becker, T.M., Grava, C., 2017. Detection of a Hydrogen Corona in HST Lyα Images of Europa in Transit of Jupiter. Astron. J. 153, 67. doi:10.3847/1538-3881/153/2/67.
Roth, L., Retherford, K.D., Saur, J., Strobel, D.F., Feldman, P.D., McGrath, M.A., Nimmo, F., 2014. Orbital apocenter is not a sufficient condition for HST/STIS detection of Europa's water vapor aurora. Proc. Natl. Acad. Sci. 111, E5123–E5132. doi:10.1073/pnas.1416671111.
Roth, L., Saur, J., Retherford, K.D., Strobel, D.F., Feldman, P.D., McGrath, M.A., Spencer, J.R., Blöcker, A., Ivchenko, N., 2016. Europa's far ultraviolet oxygen aurora from a comprehensive set of HST observations. J. Geophys. Res. (Space Phys.) 121, 2143–2170. doi:10.1002/2015JA022073.
Rubin, M., Jia, X., Altwegg, K., Combi, M.R., Daldorff, L.K.S., Gombosi, T.I., Khurana, K., Kivelson, M.G., Tenishev, V.M., Tóth, G., Holst, B., Wurz, P., 2015. Self-consistent multifluid MHD simulations of Europa's exospheric interaction with Jupiter's magnetosphere. J. Geophys. Res. 120, 3503–3524. doi:10.1002/2015JA021149.
Saur, J., Feldman, P. D., Roth, L., Nimmo, F., Strobel, D. F., Retherford, K. D., McGrath, M. A., Schilling, N., Gérard, J.-C., Grodent, D., 2011. HST/ACS observations of Europa's atmospheric UV emission at eastern elongation. ArXiv:1106.1409.
Saur, J., Strobel, D.F., Neubauer, F.M., 1998. Interaction of the Jovian magnetosphere with Europa: constraints on the neutral atmosphere. J. Geophys. Res. 103, 19947–19962. doi:10.1029/97JE03556.
Shematovich, V.I., Johnson, R.E., Cooper, J.F., Wong, M.C., 2005. Surface-bounded atmosphere of Europa. Icarus 173, 480–493.
Shi, J., Raut, U., Kim, J.-H., Loeffler, M., Baragiola, R.A., 2011. Ultraviolet photon-induced synthesis and trapping of H_2O_2 and O_3 in porous water ice films in the presence of ambient o_2: implications for extraterrestrial ice. Astrophys. J. Lett. 738, L3. doi:10.1088/2041-8205/738/1/L3.
Sittler, E.C., Strobel, D.F., 1987. Io plasma torus electrons – Voyager 1. J. Geophys. Res. 92, 5741–5762. doi:10.1029/JA092iA06p05741.
Smyth, W.H., Marconi, M.L., 2006. Europa's atmosphere, gas tori, and magnetospheric implications. Icarus 181, 510–526. doi:10.1016/j.icarus.2005.10.019.
Spencer, J.R., Calvin, W.M., 2002. Condensed O_2 on Europa and Callisto. Astrophys. J. 124, 3400–3403.
Spencer, J.R., Tamppari, L.K., Martin, T.Z., Travis, L.D., 1999. Temperatures on Europa from Galileo photopolarimeter-radiometer: nighttime thermal anomalies. Science 284, 1514. doi:10.1126/science.284.5419.1514.
Straub, H.C., Renault, P., Lindsay, B.G., Smith, K.A., Stebbings, R.F., 1996. Absolute partial cross sections for electron-impact ionization of H_2, N_2, and O_2 from threshold to 1000 eV. Phys. Rev. A 54, 2146–2153. doi:10.1103/PhysRevA.54.2146.
Tawara, H., Itikawa, Y., Nishimura, H., Yoshino, M., 1990. Cross sections and related data for electron collisions with hydrogen molecules and molecular ions. J. Phys. Chem. Ref. Data 19, 617–636. doi:10.1063/1.555856.
Teolis, B. D., Loeffler, M. J., Raut, U., Famá, M., Baragiola, R. A., Ozone synthesis on the icy satellites. Astrophys. J.
Teolis, B.D., Plainaki, C., Cassidy, T.A., Raut, U., 2017. Water ice radiolytic O_2, H_2, and H_2O_2 yields for any projectile species, energy, or temperature: A model for icy astrophysical bodies. J. Geophys. Res.: Planet. 122, 1996–2012. doi:10.1002/2017JE005285.
Tully, C., Johnson, R.E., 2001. Low energy collisions between ground-state oxygen atoms. Planet. Space Sci. 49, 533–537. doi:10.1016/S0032-0633(01)00002-2.
Wahlund, J.-E., the JUICE-RPWI team, 2013. The radio and plasma wave investigation (RPWI) for JUICE. in: Proceedings of the European Planetary Science Congress 2013, held 8–13 September, London, UK 8, 637.
Wurz, P., Lammer, H., 2003. Monte-Carlo simulation of mercurys exosphere. Icarus 164, 1–13. doi:10.1016/S0019-1035(03)00123-4.
Wurz, P., Vorburger, A., Galli, A., Tulej, M., Thomas, N., Alibert, Y., Barabash, S., Wieser, M., Lammer, H., 2014. Measurement of the Atmospheres of Europa, Ganymede, and Callisto. European Planetary Science Congress 9 EPSC2014-504.
Zheng, W., Jewitt, D., Kaiser, R.I., 2006. Formation of hydrogen, oxygen, and hydrogen peroxide in electron-irradiated crystalline water ice. Astroshys. J. 639, 534–548. doi:10.1086/499231.